Moments of inertia for multiquasiparticle configurations

S. Frauendorf,[1] K. Neergård,[2] J. A. Sheikh,[3,4] and P. M. Walker[3]
[1]*Department of Physics, University of Notre Dame, Notre Dame, Indiana 46556*
[2]*Næstved Gymnasium og HF, Nygårdsvej 43, 4700 Næstved, Denmark*
[3]*Department of Physics, University of Surrey, Guildford, Surrey GU2 5XH, United Kingdom*
[4]*Tata Institute of Fundamental Research, Bombay 400 005, India*
(Received 23 August 1999; published 23 May 2000)

Tilted-axis cranking calculations have been performed for multiquasiparticle states in well-deformed $A \approx 180$ nuclei. In the limit of zero pairing, not only are the calculated moments of inertia substantially smaller than for rigid rotation, but also they are close to the experimental values. The moments of inertia are found to be insensitive to dynamic pair correlations.

PACS number(s): 21.10.Re, 21.30.Fe, 21.60.Ev, 27.70.+q

I. INTRODUCTION

The moments of inertia of deformed atomic nuclei at low spins are a factor of 2 or 3 smaller than the rigid-body value. The reduction is attributed to the strong pair correlations, because nuclei in the ground state are in a superfluid condensed state [1]. Angular momentum is generated by either rotating the deformed superfluid or by breaking Cooper pairs from this condensed state. In order to reach high spins, an increasing number of Cooper pairs are broken, which reduces and finally quenches the pair condensate. It has been often stated that after this transition, the moments of inertia should reach the rigid-body value [1,2]. However, this conjecture is based on the consideration of two special cases [1,2]: (i) the limit of large particle number, where the nuclear shell structure becomes unimportant; and (ii) nucleons in a harmonic oscillator potential at its equilibrium deformation.

Particularly for independent particles in a harmonic oscillator potential well, the moment of inertia has in the limit of vanishing angular velocity exactly the rigid-body value in any combination of stationary single-particle states provided the total energy is stationary with respect to volume-conserving variations of the equipotential ellipsoids [3]. At finite angular velocity, the condition for the rigid-body value is that the second moments of the density distribution should have the ratio of the squares of the axes of the oscillator-plus-centrifugal equipotential ellipsoids, which is not exactly equivalent to a stationary energy [4]. These results have led to the expectation that in real nuclei, the moment of inertia would not be very different from the rigid-body value if the pairing is quenched. This expectation was substantiated by early studies like, for example, that in Ref. [5] of more realistic single-nucleon potentials, which seemed to indicate that permitting the nuclear system to relax to an equilibrium shape generally tends to reduce deviations from the rigid-body moment of inertia due to shell structure. The validity of the aforementioned conjecture for the real nuclear potential remains, however, a continuing subject of investigation with new theoretical and experimental techniques, and so does the related question of the current distribution in a rotating nucleus [6–8].

Systematic deviations from rigid-like behavior at high angular velocity have been demonstrated for transitional nuclei in the $A \approx 110$ region [9] and discussed for superdeformed nuclei [10,11]. In the present study we address the inertial behavior of a different class of nuclear excitations: high-seniority states in well deformed $A \approx 180$ nuclei (see also the earlier work by Andersson *et al.* [12]). Recently, rotational bands have been observed in, for example, ^{178}Hf, ^{178}W and ^{179}W [13–16] that are built on configurations with up to four broken pairs (that is, seniority eight) and high K values, where K is the angular momentum with respect to the body-fixed deformation axis. It is found (see the empirical data in Fig. 1) that the moments of inertia are substantially below the rigid-body value. Furthermore, some bands deviate from the linear dependence of the angular momentum on the angular velocity, expected for the strong coupling of quasiparticles to the deformed field.

These features can be explained [17] by the persistence of pair correlations in the Lipkin-Nogami pairing model, combined with the assumption that the zero-pairing limit would result in rigid-like rotation. However, since the latter assumption is not self-evident, a microscopic determination of the moment of inertia in the zero-pairing limit is required. In the present work it is demonstrated, through tilted-axis-cranking (TAC) calculations, that the main experimental features can be understood by assuming that nucleons move in a rotating mean field with *no pairing*. The preliminary results of Ref. [18] are extended.

II. THE TILTED-AXIS-CRANKING MODEL

To describe the high-K rotational bands, involving many unpaired nucleons and predominant magnetic dipole transitions, the tilted-axis-cranking approach [19] is employed. When pairing is neglected, the nuclear state $|\omega\rangle$ considered is a uniformly rotating Slater determinant which is an eigenstate of the ''Routhian''

$$h' = h_{\mathrm{def}}(\varepsilon_2, \varepsilon_4) - \omega(j_1 \sin\vartheta + j_3 \cos\vartheta), \qquad (1)$$

where h_{def} is the Hamiltonian of independent nucleons in a deformed potential, ω is the angular velocity, j_1 and j_3 are the components of the angular momentum with respect to the principal axes 1 and 3 (symmetry axis) of the deformed potential, and ϑ is the angle of the angular velocity with the 3

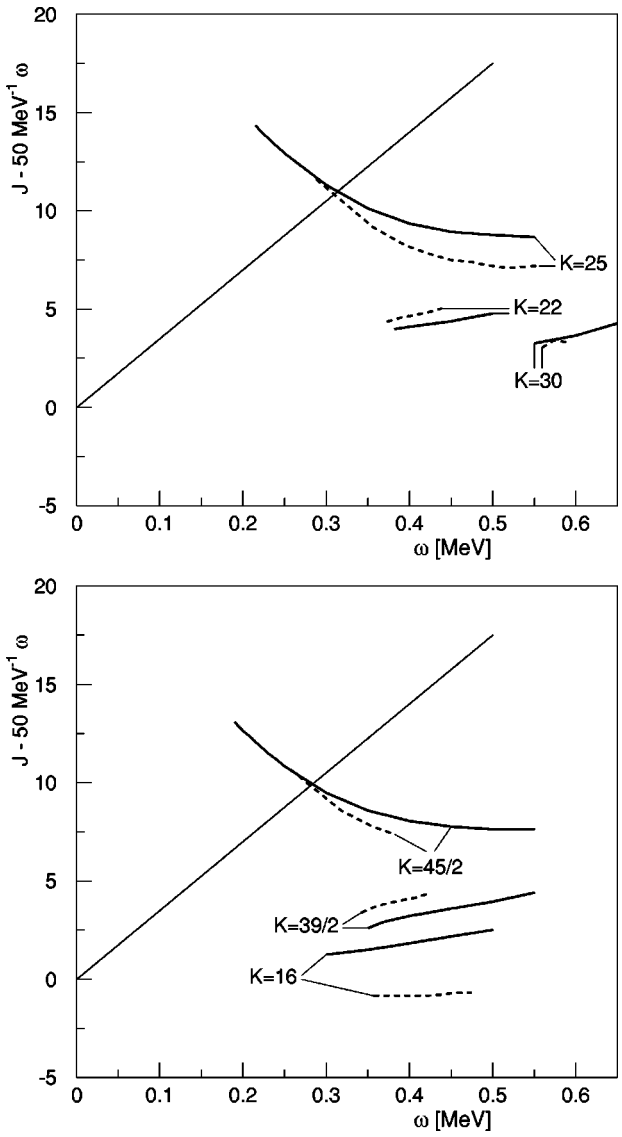

FIG. 1. Functions $J(\omega)$ calculated without pairing for several configurations listed in Table I. The value of J is given relative to a linear reference 50 MeV$^{-1}\omega$. Solid line: TAC calculation. Dashed line: experiment [13–16]. Upper panel: bands in ^{178}W. Lower panel: bands in ^{178}Hf and ^{179}W. Moments of inertia can be obtained from the graphs, as J/ω (kinematic value) and $dJ/d\omega$ (dynamic value). The straight line corresponds to the rigid moment of inertia $\mathcal{J}=85$ MeV^{-1}.

axis. The total Routhian E' is obtained by applying the Strutinsky renormalization to the energy of the nonrotating system E_0. This kind of approach has turned out to be a quite reliable calculation scheme in the case of standard cranking [20]. Thus we have

$$E'(\omega,\vartheta,\varepsilon_2,\varepsilon_4)=E_{LD}(\varepsilon_2,\varepsilon_4)-\tilde{E}+\langle\omega|h'|\omega\rangle. \qquad (2)$$

By means of Strutinsky-averaging [21], the smooth energy $\tilde{E}$ is calculated from the nonrotating single-nucleon energies, obtained from the Hamiltonian $h_{\rm def}(\varepsilon_2,\varepsilon_4)$.

The orientation angle ϑ is found by requiring the total angular momentum $\vec{J}=\langle\omega|\vec{j}|\omega\rangle$ to be parallel to $\vec{\omega}$. This makes E' a minimum with respect to ϑ. In the case of the high-K bands we are interested in, the rotational axis is ''tilted,'' i.e., it does not coincide with one of the principal axes of the deformed potential ($\vartheta\neq 90°$ or $0°$). The equilibrium shape is found by minimizing E' with respect to the deformation parameters ε_2 and ε_4 of the potential.

The calculated angular momentum $J(\omega)=\sqrt{J_1^2+J_3^2}$ is compared with the experimental function, which is constructed by the standard procedure: In terms of the energy levels $E(I)$ of a $\Delta I=1$ rotational band, where I denotes the angular momentum quantum number, one sets $\omega(J)=E(I)-E(I-1)$ for $J=I$. For a given observed band, this defines a discrete set of empirical pairs of J and ω from which the experimental function $J(\omega)$ is obtained by interpolation. [Taking $\omega(J)$ at $J=(I-\frac{1}{2})+\frac{1}{2}=I$ simulates a random-phase approximation (RPA) correction to the Hartree-Fock energy [22].]

III. SINGLE-NUCLEON HAMILTONIAN AND DEFORMATIONS

In the present calculation for the nuclei ^{178}Hf, ^{178}W, and ^{179}W, the modified oscillator form [21] of the Hamiltonian $h_{\rm def}$ was adopted. For the combinations of single-nucleon states listed in Table I, the equilibrium shape at zero angular velocity was determined. Most of the configurations in ^{178}W and ^{179}W were found to have equilibrium values of the quadrupole deformation ε_2 and hexadecapole deformation ε_4 (see Ref. [21]) close to $\varepsilon_2=0.23$ and $\varepsilon_4=0.02$. Only the $K^\pi=45/2^-$ and 25^+ configurations, which have a proton in the $1h_{9/2}$ state, have somewhat larger equilibrium deformations, given approximately by $\varepsilon_2=0.25$ and $\varepsilon_4=0.015$. In the $K^\pi=16^+$ configuration in ^{178}Hf, the equilibrium shape has $\varepsilon_2=0.22$ and $\varepsilon_4=0.05$. These values of the shape parameters were used in the following calculations. The difference between the deformation of the $K^\pi=45/2^-$ and 25^+ configurations and that of the other configurations in ^{178}W and ^{179}W changes the rigid-body moment of inertia by 6 %.

For the $K^\pi=45/2^-$ and 25^+ configurations, we studied the change of equilibrium shape as a function of the angular velocity. In the relevant interval of ω, the variation of ε_2 stays below 0.005 and that of ε_4 is negligible. This corresponds to a 2 % variation of the rigid-body moment of inertia.

IV. RESULTS AND DISCUSSION

Figure 1 shows the calculated and empirical functions $J(\omega)$ for the configurations in Table I except those with $K^\pi=7^-$ and 15^+. A close correspondence between calculation and data is apparent from this figure. This includes recent data for a $K^\pi=30^+$ band in ^{178}W [15]. It is also evident that the moments of inertia are considerably smaller than the rigid-body value, which is about 85 MeV^{-1} for these masses and shapes. The typical empirical moment of inertia is about 55 MeV^{-1}. The $K^\pi=45/2^-$ and 25^+ bands are discussed later.

TABLE I. Configurations and pair gaps for $\omega=0$ of the rotational bands discussed in this paper. The states are labeled by their angular momentum K with respect to the 3 axis and their parity π. Indicated is the composition relative to the ^{178}Hf or ^{178}W ground state in the absence of pairing, as well as the contribution to K^π of each kind of nucleon. The $K^\pi=16^+$ band belongs to the nucleus ^{178}Hf, the $K^\pi=7^+$, 15^+, 22^-, 25^+, and 30^+ bands to the nucleus ^{178}W, and the $K^\pi=39/2^+$ and $45/2^-$ bands to the nucleus ^{179}W. The orbitals are identified by their contribution to K^π. Holes are understood to occupy the time-reversed orbital. The asymptotic quantum numbers are for the proton orbitals: [514 9/2], [404 7/2], [541 1/2], [402 5/2], [505 11/2], and for the neutron orbitals: [514 7/2], [633 7/2], [642 9/2], [512 5/2]. Note that the $K^\pi=1/2^-$ proton orbital intrudes from the $1h_{9/2}$ spherical level. For each kind of nucleon, the BCS and, in a bracket, Lipkin-Nogami pair gaps calculated for $\omega=0$ are given.

K^π	Proton configuration	Δ_p (MeV)	Neutron configuration	Δ_n (MeV)
7^-	$[\ ]_{0^+}$	1.13	$[7/2^-,(7/2^+)^{-1}]_{7^-}$	0.48
15^+	$[9/2^-,(7/2^+)^{-1}]_{8^-}$	0(0.75)	$[7/2^-,(7/2^+)^{-1}]_{7^-}$	0.48
$39/2^+$	$[9/2^-,(7/2^+)^{-1}]_{8^-}$	0(0.75)	$[9/2^+,7/2^-,(7/2^+)^{-1}]_{23/2^-}$	0(0.75)
22^-	$[9/2^-,(7/2^+)^{-1}]_{8^-}$	0(0.75)	$[9/2^+,7/2^-,(5/2^-,7/2^+)^{-1}]_{14^+}$	0(0.51)
$45/2^-$	$[1/2^-,9/2^-,(5/2^+,7/2^+)^{-1}]_{11^+}$	0(0.66)	$[9/2^+,7/2^-,(7/2^+)^{-1}]_{23/2^-}$	0(0.75)
25^+	$[1/2^-,9/2^-,(5/2^+,7/2^+)^{-1}]_{11^+}$	0(0.66)	$[9/2^+,7/2^-,(5/2^-,7/2^+)^{-1}]_{14^+}$	0(0.51)
30^+	$[11/2^-,9/2^-,(5/2^+,7/2^+)^{-1}]_{16^+}$	0	$[9/2^+,7/2^-,(5/2^-,7/2^+)^{-1}]_{14^+}$	0
16^+	$[9/2^-,(7/2^+)^{-1}]_{8^-}$	0(0.84)	$[7/2^-,(9/2^+)^{-1}]_{8^-}$	0(0.77)

This strong deviation from the behavior of the moment of inertia in the limit of large particle number [1,2] may be understood from the details of the shell structure at prolate deformation. Thus, the upper and middle parts of the 50–82 proton and 82–126 neutron shells, where the Fermi levels are situated in these nuclei (with $Z=72,74$ and $N=104$–106), have a concentration of orbitals that are strongly coupled to the deformed potential. This inhibits the generation of total angular momentum by alignment of the angular momenta of the individual nucleons with the 1 axis. The result is a moment of inertia that is smaller than the average. The effect is illustrated by Fig. 2, which shows that in comparison with the weakly coupled $1h_{9/2}$ proton orbital, the angular momentum of the strongly coupled orbitals tends to stay closely aligned with the 3 axis, and for some orbitals even slightly antialigned with the 1 axis.

In contrast, moments of inertia above the average are expected for nuclei with Fermi levels in the lower parts of the major shells. Such a variation was actually found through the 82–126 neutron shell in the detailed calculations in Ref. [5]. With increasing deformation, the shell structure, and hence its contribution to the moment of inertia, is progressively damped [5]. Less pronounced deviations from the rigid-body value are, therefore, expected for superdeformed nuclei.

It should be noted that the substantial deviations from the rigid-body moment of inertia seen in Fig. 1 occur at the calculated equilibrium shape of each configuration. A similar experience applies to the magnetic susceptibility of small metal clusters [23], which have a flat-bottom single-particle potential like that of atomic nuclei. The deviation from the rigid-body moment of inertia reflects a nonrigid flow of mass in the rotational states. Such intrinsic mass currents have been discussed for atomic nuclei by several authors [6–8] as well as for small metal clusters [23].

The behavior of the $K^\pi=16^+$, $39/2^+$, 22^- and 30^+ bands is well described in terms of a constant moment of inertia of each configuration with a value about 55 MeV^{-1}. Such a constant moment of inertia corresponds to the familiar expression for the energy levels in a rotational band built on a strongly coupled intrinsic state, $E(I)=[I(I+1)-K^2]/2\mathcal{J}$, and it indicates a collective origin of the angular momentum with respect to the 1 axis.

The $K^\pi=45/2^-$ and 25^+ bands show a totally different behavior with a large up-curvature of the function $J(\omega)$. Asymptotically, in the limit of large angular velocity, the moments of inertia approach values similar to those of the other

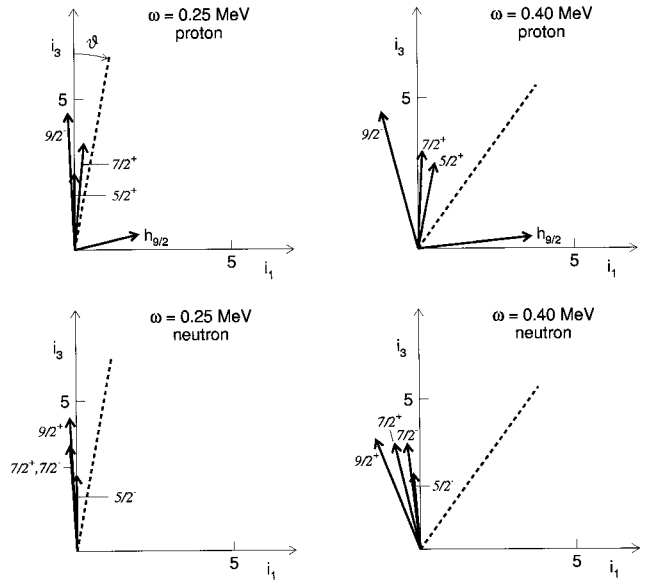

FIG. 2. The vectors $(i_1,i_3)=\langle(j_1,j_3)\rangle$ of the active particles in the $K^\pi=25^+$ band. They are calculated for the eigenstates of the Routhian (1) without pairing at $\omega=0.25$ MeV and $\omega=0.40$ MeV and the corresponding tilt angle ϑ. For each vector the label K^π corresponds to the one in Table I, except that $h_{9/2}$ corresponds to $1/2^-$ in the table. The dashed line shows the common direction of the vectors $\vec{\omega}$ and $\vec{J}$, which is tilted by the angle ϑ from the 3 axis.

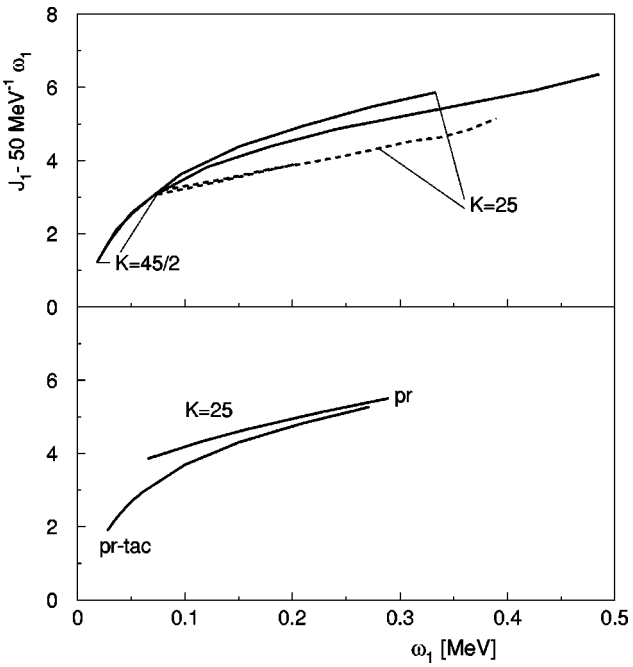

FIG. 3. Functions $J_1(\omega_1)$ for the $K^\pi = 45/2^-$ and 25^+ bands. The value of J_1 is given relative to a linear reference 50 $\mathrm{MeV}^{-1}\omega_1$. The upper panel shows the experiment [14–16] (dashed) and the TAC calculations (solid), which are without pairing. Note that these calculations and data are the same as those in Fig. 1. They are just presented differently. The lower panel shows the results of the schematic model discussed in Sec. V C. Labels: pr-tac indicates the cranking case, pr indicates the quantal case.

bands. As discussed in Ref. [17], this behavior results from the presence of a $1h_{9/2}$ proton orbital in the configurations of the $K^\pi = 45/2^-$ and 25^+ bands. In fact, as the component ω_1 of the angular velocity becomes finite, this weakly coupled orbital, which intrudes from the the $Z = 82$–126 spherical shell, immediately aligns its angular momentum with the 1 axis, thus making a significant contribution to the component J_1 of the total angular momentum on the 1 axis. The situation is illustrated in Fig. 2.

The functions $J_1(\omega_1)$ actually calculated for these two bands are shown in Fig. 3. Corresponding empirical functions were extracted from the data by assuming, in close accordance with what is calculated, that J_3 is constant and equal to K, i.e.,

$$J_1 = \sqrt{J^2 - K^2}, \quad \omega_1 = \omega\sqrt{1-(K/J)^2}. \tag{3}$$

In the empirical range of ω_1, both the calculated and the measured functions are seen to be fairly linear, and extrapolating these parts of the curves to $\omega_1 = 0$ yields the common value $J_1 = 2.8 \pm 0.5$ (cf. Fig. 3).

In order to see how the behavior of the $K^\pi = 45/2^-$ and 25^+ bands seen in Fig. 1 may emerge from this picture, consider an idealized scenario where the $1h_{9/2}$ proton orbital makes a constant contribution i to J_1, and all orbitals together a constant contribution to J_3 equal to K and a contribution to J_1 equal to $\mathcal{J}_R\omega_1$, where $\mathcal{J}_R$ is a constant. (Such a schematic model is discussed in more detail in Sec. V C.) With $J_1 = \mathcal{J}_R\omega_1 + i$ and Eq. (3), we have

$$\omega = \left(1 - \frac{i}{\sqrt{J^2-K^2}}\right)\omega_{\mathrm{sc}}, \quad \omega_{\mathrm{sc}} = \frac{J}{\mathcal{J}_R}, \tag{4}$$

where ω is seen to become smaller than the frequency ω_{sc} for strong coupling ($i = 0$).

In the calculation, there is a gradual increase of the contribution i to J_1 of the $1h_{9/2}$ proton orbital towards its maximum 9/2. Thus, the assumption above of a constant i was too schematic. The calculated curves show a slight down curvature due to saturation of i. The absence of a similar down curvature in the data might be the result of a counteractive nonlinearity of the remaining, collective, part of J_1. In that case, the present calculation does not get this part quite right and overestimates the collective moment of inertia by about 5 MeV^{-1}. Nevertheless, these considerations show that (i) the essential difference of behavior, induced by the alignment with the 1 axis of the angular momentum of the $1h_{9/2}$ proton, can be well understood, and (ii) the collective part $\mathcal{J}_R$ is about 55 MeV^{-1}, like for the other bands.

V. ADDITIONAL INVESTIGATIONS

The calculations for zero pairing, and their comparison with experimental data, constitute the principal outcome of this work. However, it is also instructive to investigate some finite-pairing effects and other model assumptions.

A. Static pairing

Pairing is taken into account [19] by including the pair field in the quasiparticle Routhian

$$h' = h_{\mathrm{def}} + \Delta(P^+ + P) - \lambda N - \omega(j_1 \sin\vartheta + j_3 \cos\vartheta), \tag{5}$$

where P^+ is the monopole pair operator and N is the particle number. In order to keep the notation simple we do not distinguish between the proton and neutron parts of the pair field. The rotating deformed state is obtained by replacing the Slater determinant by the quasiparticle configuration $|\omega\rangle$, which is the eigenstate of Eq. (5). The vector $\vec{J}$ is equal to $\langle\omega|\vec{j}|\omega\rangle$ with this new state $|\omega\rangle$. The chemical potential λ is fixed by requiring $\langle\omega|N|\omega\rangle$ to be equal to the actual particle number, and the pair gap Δ by the self-consistency condition $\Delta = G\langle\omega|P|\omega\rangle$. For $\Delta = 0$, this formalism is equivalent to the previous one.

The pairing force constants G_n and G_p were determined by the condition that the pair gaps in the nuclear ground state should be equal to the empirical odd-even mass differences. It is well known from previous studies (for instance, Ref. [24]) that with increasing angular velocity, the pair gaps and chemical potentials change their values essentially stepwise with a successive breaking of Cooper pairs. Since a detailed description of the paired state is not the concern of this paper, the chemical potentials and pair gaps were kept constant for each configuration as long as there was no pair breaking encountered.

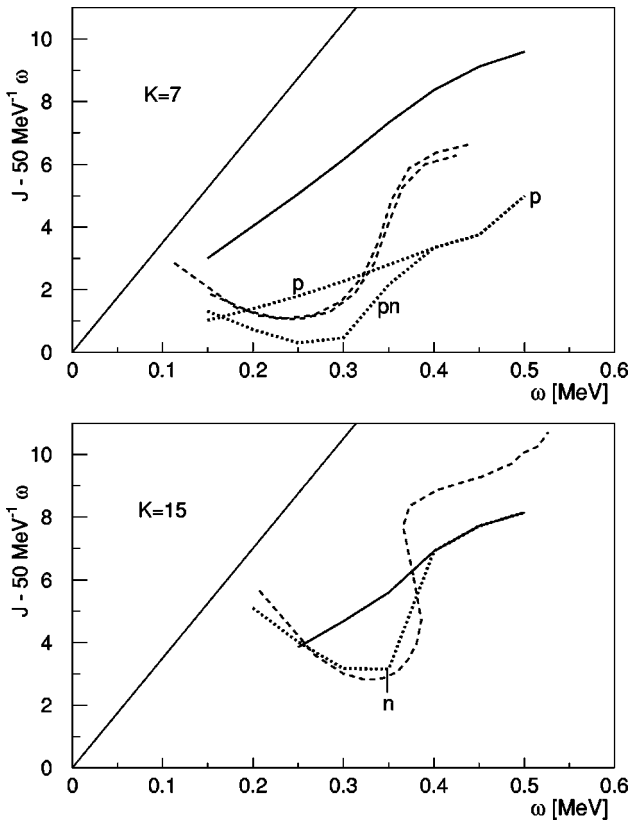

FIG. 4. Functions $J(\omega)$ calculated for the bands $K^{\pi}=7^{-}$ (upper panel) and $K^{\pi}=15^{+}$ (lower panel) with and without static pairing. Solid line: no pairing. Dotted line: with pairing. Dashed line: experiment [14,15]. The labels additionally distinguish between different combinations of the pair gaps: p: $\Delta_p=1.13$ MeV, $\Delta_n=0$; n: $\Delta_p=0$, $\Delta_n=0.48$ MeV; pn: $\Delta_p=1.13$ MeV, $\Delta_n=0.48$ MeV. The curve n in the lower panel merges with the solid line and the curve pn in the upper panel with the curve p because $\Delta_n=0$ is found for $\omega\geqslant 0.4$ MeV. The value of J is given relative to a linear reference 50 $\mathrm{MeV}^{-1}\omega$. The straight line corresponds to the rigid moment of inertia $\mathcal{J}=85$ MeV^{-1}.

The pair gaps determined at the band heads are listed in Table I. For most of the configurations, they are seen to vanish. Exceptions are the $K^{\pi}=7^{-}$ and 15^{+} states. These have a common neutron configuration with one broken Cooper pair, which leaves a reduced but finite neutron pair gap. The $K^{\pi}=7^{-}$ state furthermore has the ground-state proton configuration and hence the ground-state proton pair gap. The proton configuration of the $K^{\pi}=15^{+}$ state is found in the calculation to be just on the border of having a static proton pair field. Small variations of G_p about the value obtained by adjustment to the odd-even mass difference in fact cause Δ_p to vary between 0 and 0.5 MeV. For the calculations, we have chosen $\Delta_p=0$, as also listed in Table I. This gives a good agreement with the measured function $J(\omega)$.

Figure 4 shows the functions $J(\omega)$ calculated for the $K^{\pi}=7^{-}$ and 15^{+} bands. Both of them are seen to bend upwards near $\omega=0.35$ MeV. This is because, by breaking a Cooper pair, two neutrons in $1i_{13/2}$ orbitals align their angular momenta with the 1 axis. For $\omega\geqslant 0.4$ MeV, a vanishing pair gap is calculated for this neutron configuration. Therefore, in the figure we let the curves calculated with the neutron pair gap at the band head join for $\omega\geqslant 0.4$ MeV those calculated with $\Delta_n=0$. These are about 2 units below the measured curves in this range of ω. We could not find a reason for the discrepancy.

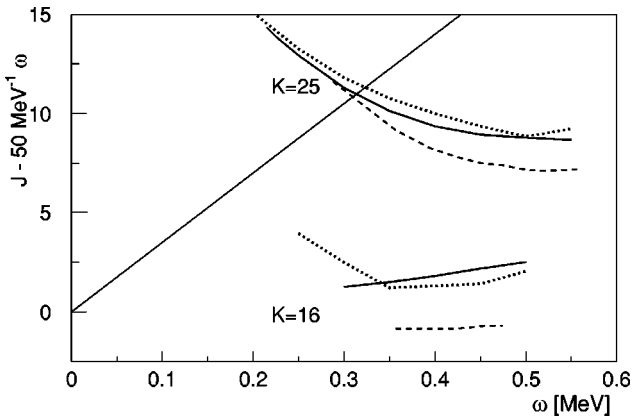

FIG. 5. Influence of the dynamical pair correlations on $J(\omega)$ for the $K^{\pi}=16^{+}$ and 25^{+} bands. Solid line indicates no pairing. Dotted line is calculated using the Lipkin-Nogami pair gaps quoted in Table I. Dashed line is the experiment [13–15]. The value of J is given relative to a linear reference 50 $\mathrm{MeV}^{-1}\omega$. The straight line corresponds to the rigid moment of inertia $\mathcal{J}=85$ MeV^{-1}.

This pair breaking is of the type known as a BC crossing (see, for example, Ref. [25]). As also seen from Fig. 4, no similar upbends arise in the case $\Delta_n=0$. This conforms to the general experience [26] that a static pair field is required for band crossings of the types AB, BC, etc. Thus, the presence of upbends in the data is evidence for a static neutron pair field in these bands.

B. Pair fluctuations

Near the critical point of the vanishing of the static pair gap, large fluctuations of the pair field, known as dynamic pair correlations, are expected [24,27]. Dynamic pair correlations are taken into account in an approximate way by the Lipkin-Nogami correction for the fluctuation of particle number in the BCS state. (See Ref. [28] and references therein.) For several configurations, we made the Lipkin-Nogami calculation at the band head. The resulting Lipkin-Nogami pair gaps are also shown in Table I. With these gaps, $J(\omega)$ was calculated as in the case of static pairing (see Sec. V A), except that the chemical potentials were adjusted with the angular velocity so as to keep the correct expectation values of the proton and neutron numbers.

The calculated functions $J(\omega)$ for the $K^{\pi}=16^{+}$ and 25^{+} bands shown in Fig. 5 are representative for the results. It is seen that relative to the calculation without pairing, the pair fields produced by the Lipkin-Nogami pair gaps make only minor corrections to the angular momentum (of the order of 1 unit), which do not improve the agreement with experiment. Thus, pair fluctuations appear to be inessential for the explanation of the observed deviations from the rigid value

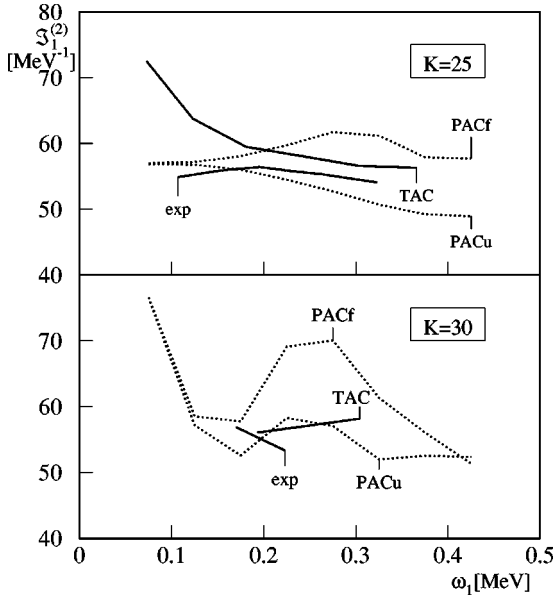

FIG. 6. Moments of inertia $dJ_1/d\omega_1$. Solid lines are the TAC calculation and experimental values [14,15]. Dotted lines are the PAC calculations, favored and unfavored bands. Upper panel is the $K^\pi=25^+$ band. Lower panel is the $K^\pi=30^+$ band. The discrepancy between the TAC calculation and the experimental data for the $K^\pi=25^+$ band at low ω_1 is discussed at the end of Sec. IV.

of the moments of inertia at high values of K.

This result may seem to be at variance with the investigation of low-K bands in Refs. [24,27]. There it was found that at frequencies where the static pair gap is zero the pair fluctuations reduce the angular momentum by 3–4 units in the yrast band of even-even nuclei. The different sensitivity to the pair correlations may be understood. In order to generate the angular momentum along the 3 axis (high K) several pairs are broken. This blocks the affected single-particle states from taking part in the pair correlations. However, it is just the contribution of these particles near the Fermi surface which is most sensitive to the pair correlations. In the case of the yrast bands of the even-even nuclei only one neutron pair $(1i_{13/2})$ is broken. Consequently these bands are more sensitive to the pair fluctuations. This argument is consistent with Refs. [24,27], where it was found that in bands with two broken pairs (odd-A nuclei and negative parity bands in even-even nuclei) the pair fluctuations reduce the angular momentum only by 1–2 units. Hence, only the low-K bands are suited to study the influence of the pair fluctuations on the moments of inertia.

C. A particle-rotor model calculation

It was seen in Sec. IV that the behavior of the $K^\pi=45/2^-$ and 25^+ bands at low angular velocity is largely determined by a single proton in a $1h_{9/2}$ orbital. The behavior was qualitatively explained in terms of a particle-rotor model where all nucleons except the $1h_{9/2}$ proton are assumed to make a constant contribution to J_3 equal to $K_R=K-\frac{1}{2}$ and a contribution to J_1 equal to $\mathcal{J}_R\omega_1$, where $\mathcal{J}_R$ is a constant. This situation may be further analyzed by calculating the quantal states of this model. In particular, we address the question of whether the deviations between the experiment and the calculation in the upper panel of Fig. 3 are related to the violation of angular momentum conservation in the TAC model. A quantal treatment of the system of a particle coupled to a $K_R\neq 0$ rotor was given previously in Ref. [29].

The coupling of the $1h_{9/2}$ proton to the deformed core is treated in a schematic way. The particle space is restricted to a multiplet of angular-momentum eigenstates with quantum number $j=9/2$, and $h_{\rm def}$, acting on the single proton, is taken to be a quadratic function of j_3. The coefficient of this quadratic function is chosen so as to reproduce the splitting of the $1h_{9/2}$ proton level found for the full Hamiltonian $h_{\rm def}$ at the deformations of the $K^\pi=45/2^-$ and 25^+ band heads (see Sec. III).

The particle-rotor problem can be treated in the semiclassical TAC approximation. The details are described in Ref. [30]. The function $J_1(\omega_1)$ of the $K^\pi=25^+$ band thus calculated with $\mathcal{J}_R=55$ MeV^{-1} is shown in the lower panel of Fig. 3. It is seen that the schematic model reproduces the result of the full TAC calculation, seen in the upper panel, very closely.

The result of the exact quantal treatment of the same particle-rotor model is also shown in the lower panel of Fig. 3. In order to generate the plot the quantal energies are treated like empirical ones (see Secs. II and IV). The quantal calculation conforms better to the data than the TAC approximation in producing a more linear function $J_1(\omega_1)$. However, extrapolating this function from the empirical range of ω_1 to $\omega_1=0$ yields $J_1=3.5$, which is significantly larger than the empirical value $J_1=2.8$.

The different behaviors of the quantal particle-rotor model and the TAC approximation to it arise essentially from replacing the recoil energy $(j_1^2+j_2^2)/2\mathcal{J}_R$ by $\langle j_1\rangle^2/2\mathcal{J}_R$ [30]. While the former is approximately a constant, the latter acts as a potential that hinders the increase of $\langle j_1\rangle$. Contrary to the quantal model, the cranking model was seen to reproduce the extrapolated value of J_1 found empirically for the $K^\pi=45/2^-$ and 25^+ bands. Thus, the nuclear system does not seem to absorb the recoil angular momentum of the $1h_{9/2}$ proton into just a single degree of freedom, as assumed in the quantal particle-rotor model. The present study does not provide an answer to the interesting question: How can the experimental curve $J_1(\omega_1)$ be so strikingly linear while the alignment is far from being complete?

D. How important is tilting the cranking axis?

In the standard principal-axis cranking (PAC) model, $\omega_3=0$ is assumed. Thus, one obtains a function $J_1(\omega_1)$. A corresponding empirical function is extracted from the data by combining the TAC geometry with the assumption $J_3=K=$constant for a rotational band with a band head angular-momentum quantum number K [31]. What makes the essential difference between the PAC and TAC models is thus the term $-\omega_3 j_3$ in the Routhian (1) of the latter. This term violates the invariance under rotation by the angle 180° about the 1-axis, whose eigenvalue is the ''signature.'' In the PAC

model, a ''favored'' and an ''unfavored'' function $J_1(\omega_1)$, where the latter is the larger, are associated with a configuration with $K \neq 0$. These functions have opposite signature and correspond to two separate level sequences with $\Delta I = 2$.

Derivatives $dJ_1/d\omega_1$ for the $K^\pi = 25^+$ and 30^+ bands calculated in both models are compared with the corresponding empirical data in Fig. 6. The derivative is seen to depend much more violently on ω_1 in the PAC model than in the TAC model. Furthermore, the PAC calculation shows a substantial signature splitting. Since neither of these features is seen in the data, it must be concluded that the term $-\omega_3 j_3$ in the Routhian (1) is significant for the description of these high K bands. The difference between the PAC and TAC results is larger for the $K^\pi = 30^+$ than the $K^\pi = 25^+$ band. This is due to the smaller deformation ε_2 of the former.

VI. CONCLUSION

It has been shown quantitatively how the moments of inertia in the zero-pairing limit may be substantially lower than the rigid-body value, indicating the presence of mass currents of quantal origin in the body-fixed frame of reference. Lower-than-rigid moments of inertia are both calculated and observed systematically for rotational bands in ^{178}Hf, ^{178}W, and ^{179}W, where the neutron and proton Fermi levels are in the mid-to-upper portions of their respective shells. The analysis of a number of high-seniority bands shows that they behave as if the nuclei rotate in the unpaired state. The limited sensitivity of the calculated multiquasiparticle rotational motion to pair gaps in the range 0–50 % of their full value suggests that moments of inertia of high-K bands may not be significantly affected by dynamic pair correlations.

ACKNOWLEDGMENTS

This work was supported in part by the U.K. Engineering and Physical Sciences Research Council and by U.S. DOE Grant No. DE-FG02-95ER40934.

[1] A. Bohr and B. R. Mottelson, *Nuclear Structure*, Vol. II (Benjamin, New York, 1975), p. 78.
[2] P. Ring and P. Schuck, *The Nuclear Many Body Problem* (Springer, Berlin, 1980), p. 131.
[3] A. Bohr and B. R. Mottelson, Mat. Fys. Medd. K. Dan. Vidensk. Selsk. **30**(1), 1 (1955).
[4] J. G. Valatin, Proc. R. Soc. London, Ser. A **238**, 132 (1956).
[5] V. V. Pashkevich and S. Frauendorf, Yad. Fiz. **20**, 1122 (1975) [Sov. J. Nucl. Phys. **20**, 588 (1975)].
[6] M. Radomski, Phys. Rev. C **14**, 1704 (1976).
[7] G. Gneuss and W. Greiner, Nucl. Phys. **A171**, 449 (1971).
[8] M. Durand, P. Schuck, and J. Kunz, Nucl. Phys. **A439**, 263 (1985).
[9] R. Wadsworth, C. W. Beausang, M. Cromaz, J. DeGraaf, T. E. Drake, D. B. Fossan, S. Flibotte, A. Galindo-Uribarri, K. Hauschild, I. M. Hibbert, G. Hackman, J. R. Hughes, V. P. Janzen, D. R. LaFosse, S. M. Mullins, E. S. Paul, D. C. Radford, H. Schnare, P. Vaska, D. Ward, J. N. Wilson, and I. Ragnarsson, Phys. Rev. C **53**, 2763 (1996).
[10] I. Ragnarsson, Phys. Lett. B **199**, 317 (1987).
[11] T. Bengtsson, I. Ragnarsson, and S. Aberg, Phys. Lett. B **208**, 39 (1988).
[12] C. G. Anderssen, J. Krumlinde, G. Leander, and Z. Szymanski, Nucl. Phys. **A361**, 147 (1981).
[13] S. M. Mullins, G. D. Dracoulis, A. P. Byrne, T. R. McGoram, S. Bayer, W. A. Seale, and F. G. Kondev, Phys. Lett. B **393**, 279 (1997).
[14] C. S. Purry, P. M. Walker, G. D. Dracoulis, T. Kibédi, S. Bayer, A. M. Bruce, A. P. Byrne, M. Dasgupta, W. Gelletly, F. Kondev, P. H. Regan, and C. Thwaites, Phys. Rev. Lett. **75**, 406 (1995); C. S. Purry, P. M. Walker, G. D. Dracoulis, T. Kibédi, F. G. Kondev, S. Bayer, A. M. Bruce, A. P. Byrne, W. Gelletly, P. H. Regan, C. Thwaites, O. Burglin, and N. Rowley, Nucl. Phys. **A632**, 229 (1998).
[15] D. M. Cullen, S. L. King, A. T. Reed, J. A. Sampson, P. M. Walker, C. Wheldon, F. Xu, G. D. Dracoulis, L.-Y. Lee, A. O. Machiavelli, R. W. MacLeod, A. N. Wilson, and C. Barton, Phys. Rev. C **60**, 064301 (1999).
[16] P. M. Walker, G. D. Dracoulis, A. P. Byrne, T. Kibédi, B. Fabricius, A. E. Stuchbery, and N. Rowley, Nucl. Phys. **A568**, 397 (1994).
[17] G. D. Dracoulis, F. G. Kondev, and P. M. Walker, Phys. Lett. B **419**, 7 (1998).
[18] S. Frauendorf, in *Proceeding of the Workshop on Gamma-sphere Physics*, Berkeley, 1995 (World Scientific, Singapore, 1996), p. 272.
[19] S. Frauendorf, Nucl. Phys. **A557**, 469c (1993).
[20] T. Bengtsson and I. Ragnarsson, Nucl. Phys. **A436**, 14 (1985).
[21] S. G. Nilsson and I. Ragnarsson, *Shapes and Shells in Nuclear Structure* (Cambridge University Press, Cambridge, 1995).
[22] E. R. Marshalek, Nucl. Phys. **A275**, 416 (1977).
[23] S. Frauendorf, S. Reimann, and V. V. Pashkevich, Surf. Rev. Lett. **3**, 441 (1996).
[24] Y. R. Shimizu, J. D. Garrett, R. A. Broglia, M. Gallardo, and E. Vigezzi, Rev. Mod. Phys. **61**, 131 (1989).
[25] M. J. A. de Voigt, J. Dudek, and Z. Szymanski, Rev. Mod. Phys. **55**, 949 (1983).
[26] S. Frauendorf, Nucl. Phys. **A409**, 243c (1983).
[27] R. A. Broglia, M. Diebel, S. Frauendorf, and M. Gallardo, Phys. Lett. **166B**, 252 (1986).
[28] W. Nazarewicz, M. A. Riley, and J. D. Garrett, Nucl. Phys. **A512**, 61 (1990).
[29] K. Neergård, P. Vogel, and M. Radomski, Nucl. Phys. **A238**, 199 (1975).
[30] S. Frauendorf and J. Meng, Nucl. Phys. **A617**, 131 (1997).
[31] R. Bengtsson and S. Frauendorf, Nucl. Phys. **A327**, 139 (1979).